Supramolecular Biomaterials

DOI: 10.1002/anie.201100202

Electrostatic Control of Bioactivity**

*Joshua E. Goldberger, Eric J. Berns, Ronit Bitton, Christina J. Newcomb, and Samuel I. Stupp**

Understanding of how to design artificial extracellular matrices that effectively signal and direct cellular responses is essential for the creation of new therapies in regenerative medicine.[1] Injectable, self-assembling biomaterials capable of forming scaffolds in situ around cells are promising therapeutic candidates because of their minimally invasive delivery.[1c,2] The signaling efficacy of self-assembling bioactive structures will depend not only on molecular structure but also on nanoscale morphology.[1b,3] Peptide amphiphiles (PAs; Scheme 1) are a class of molecules that spontaneously self-assemble into a variety of nanostructures, including spherical micelles, fibers, and ribbons, and have shown promising therapeutic functions.[1c,4] Fibers have been found to be particularly bioactive. PA molecules that form fibers consist typically of four main segments: 1) a hydrophobic group, commonly an alkyl tail, that drives aggregation through hydrophobic collapse; 2) a β-sheet-forming peptide that promotes nanofiber formation; 3) a peptide segment that contains ionizable side-chain residues; and 4) a signaling moiety designed to interact with cellular receptors. These molecules self-assemble into high-aspect-ratio nanofibers that form gels in water at low concentrations when the charges on the ionic side chains are appropriately screened. These cylindrical nanofibers display bioactive sequences perpendicular to their long axis at near van der Waals density.[5]

We have shown that PAs containing the laminin-derived pentapeptide IKVAV can induce differentiation of neural stem cells into neurons, promote neurite outgrowth, and lead to functional improvement after acute spinal-cord injury.[5,6] Therefore, structures containing this epitope could also have a profound impact on regenerative therapies requiring new neurons, such as Parkinson's and Alzheimer's disease, and also help to repair brain tissue following trauma or stroke. The IKVAV epitope has been shown to bind to at least two receptors, a 110 kDa laminin-binding protein (LBP110/APP) and nucleolin,[7] although the exact molecular arrangement of this binding and the signal-transduction pathways have yet to be elucidated. This IKVAV pentamer contains mostly amino acids with hydrophobic residues that have a strong β-sheet propensity,[8] and peptides containing this epitope have a strong tendency to form amyloid-like fibrils.[9] If this IKVAV segment were to exist in a rigid β-sheet conformation with neighboring epitopes, its ability to bind to the target receptor would be highly restricted. In fact, in previous studies on IKVAV covalently grafted to polymer scaffolds, enhanced neurite outgrowth and neuronal differentiation were not observed,[10] possibly as a result of ineffective epitope presentation. Consequently, an effective supramolecular strategy to control the epitope presentation of this and other hydrophobic bioactive signals is required to enhance the signal transduction of biomaterials.

We report herein a design strategy that utilizes electrostatics to control the assembly behavior of PA molecules containing the hydrophobic IKVAV epitope. The PAs in this study contain a palmitic acid tail, a VVAA β-sheet-forming region, different numbers of charged glutamic acid residues and glycine residues, and IKVAV (Scheme 1). The key element of the design is the increased number of charged amino acid residues preceding the IKVAV segment, to reduce the propensity for epitope aggregation. PAs were synthesized by solid-phase Fmoc synthesis (Fmoc = 9-fluorenylmethoxy-

[*] Dr. J. E. Goldberger,[#] [+] Prof. S. I. Stupp
Department of Chemistry, Northwestern University
Evanston, IL 60208 (USA)
Fax: (+1) 847-491-3010
E-mail: s-stupp@northwestern.edu
E. J. Berns[+]
Department of Biomedical Engineering, Northwestern University
Evanston, IL 60208 (USA)
Dr. R. Bitton
Institute for BioNanotechnology in Medicine
Northwestern University, Chicago, IL 60611 (USA)
C. J. Newcomb, Prof. S. I. Stupp
Department of Materials Science and Engineering
Northwestern University, Evanston, IL 60208 (USA)
Prof. S. I. Stupp
Feinberg School of Medicine, Northwestern University
Evanston, IL 60208 (USA)
[#] Current address:
Department of Chemistry, The Ohio State University
Columbus, OH 43210 (USA)
[+] These authors contributed equally.

[**] The authors acknowledge James Hulvat, Liam Palmer, Hongang Cui, Shantanu Sur, and Sunitha Suresh for helpful discussions. We acknowledge the following Northwestern University facilities: IBNAM Peptide Core, IBNAM Cleanroom Core, Keck, BIF, MRC, Cell Imaging Facility (generously supported by NCI CCSG P30 CA060553 awarded to the Robert H. Lurie Comprehensive Cancer Center), C. Shad Thaxton laboratory (DLS), J. B. Cohen X-Ray Diffraction Facility. We acknowledge financial support by the MRSEC program and the National Science Foundation (DMR-0520513).WAXS was carried out at the Argonne National Laboratory at the BioCARS 14-BM-C beamline. Additional support from the Ben Gurion University in Negev, Israel in the form of a postdoctoral fellowship for R.B. is also acknowledged. This project was supported by the Army Research Office (W911NF-09-1-0044) and the National Institute of Biomedical Imaging and Bioengineering (Award Numbers F32EB007131 and 5 R01EB003806-05). The content is solely the responsibility of the authors and does not necessarily represent the official views of the National Institute of Biomedical Imaging and Bioengineering or the National Institutes of Health.

Supporting information for this article, including detailed synthetic and purification procedures, peptide-content analysis, high-resolution mass spectrometry, molecular simulations, WAXS analysis, calculation of the percentage of nanostructure surface area that is not interdigitated, and the cell-culture protocol, is available on the WWW under http://dx.doi.org/10.1002/anie.201100202.

© 2011 Wiley-VCH Verlag GmbH & Co. KGaA, Weinheim

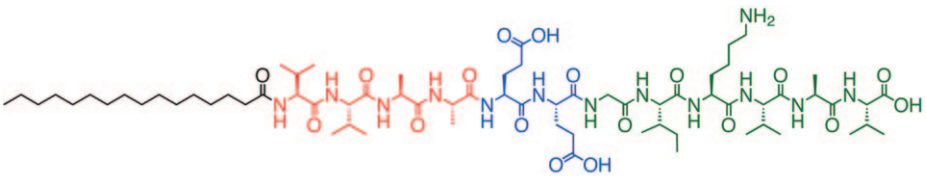

1 palmitoyl-VVAAEE-NH_2
2 palmitoyl-VVAAEEGIKVAV-COOH
3 palmitoyl-VVAAEEEGIKVAV-COOH
4 palmitoyl-VVAAEEEGGIKVAV-COOH
5 palmitoyl-VVAAEEEEGIKVAV-COOH

Scheme 1. The peptide-amphiphile design includes a hydrophobic group (black), a β-sheet-forming sequence (red), charged amino acids (blue), and a bioactive epitope (green). Peptide amphiphiles **1**–**5** were synthesized.

carbonyl) and purified by high-performance liquid chromatography (see Figure S1 in the Supporting Information). We studied the assembly of each molecule under physiologically relevant conditions by cryogenic electron microscopy (cryoTEM; Figure 1 a–d). For these experiments, PAs were dissolved in isotonic salt solutions resembling extracellular fluid (150 mM NaCl, 3 mM KCl, pH 7.4). We also used conventional transmission electron microscopy (TEM) to study the assembly of the various molecules; in this case samples were dissolved in water (Figure 1 e–h).

PA **1**, which lacks the IKVAV epitope, assembles into canonical cylindrical fibers (see Figure S2a) that have an average diameter of (6.6 ± 0.9) nm (see Figure S3). This diameter is 87% of twice the length of **1** according to MM+ molecular simulations and thus corresponds approximately to the expected diameter of cylindrical fibers consisting of hydrophobically collapsed β sheets displaying the epitope on their surfaces (Table 1). To compare molecular-simulation diameters with those observed by TEM, we scaled the molecular-simulation values by 87%. PA **2**, which incorporates the IKVAV epitope, forms ribbon morphologies in solution that are comprised of at least three cylindrical fibers of (6.0 ± 0.5) nm in diameter side by side (Figure 1 a,e). The low q region of the small-angle X-ray scattering (SAXS) curve ($q < 10^{-1}$ Å) can be fit to a ribbon morphology with a (6.0 × 18.0) nm rectangular cross-section (Figure 2 a; see also Figure S4). This result confirms that ribbons of three bundled cylindrical nanofibers are the dominant supramolecular architecture (see Figure S2b). The predicted diameter of fibers of **2** from

Table 1: Morphologies observed by TEM, simulated molecular length, scaled simulated diameter, and diameter observed by TEM for individual fibers of **1**–**5**.

PA	Assembled morphology	Simulated molecular length [Å]	Scaled, simulated diameter [Å]	Observed fiber diameter [Å]
1	cylindrical fiber	38.0	66	66 ± 9
2	trimer ribbon	55.5	97	60 ± 5
3	trimer ribbon	59.6	104	71 ± 10
3	cylindrical assembly	59.6	104	128 ± 14
4	dimer bundle	63.5	110	77 ± 9
4	triple helix	63.5	110	81 ± 10
5	cylindrical fiber	60.1	105	108 ± 15

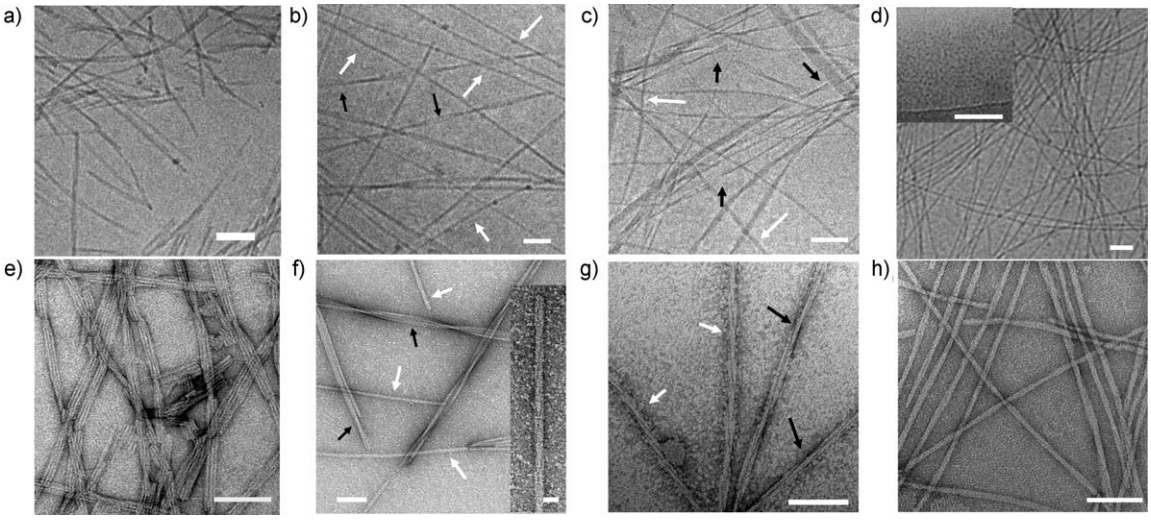

Figure 1. a–c) CryoTEM images of **2**–**4** in an isotonic salt solution containing 150 mM NaCl, 3 mM KCl. d) CryoTEM image of **5** dissolved in a salt solution containing 150 mM NaCl, 3 mM KCl, 5 mM $CaCl_2$. The inset shows a cryoTEM image of **5** in an isotonic salt solution containing 150 mM NaCl, 3 mM KCl. e–h) TEM images of **2**–**5** from solutions prepared in H_2O. In both (b) and (f), black and white arrows indicate trimer-bundle motifs and cylindrical assemblies, respectively. In both (c) and (g), black and white arrows indicate triple helices and dimer-bundle motifs, respectively. All scale bars: 100 nm, except for the inset in (f) where the scale bar is 20 nm.

 © 2011 Wiley-VCH Verlag GmbH & Co. KGaA, Weinheim

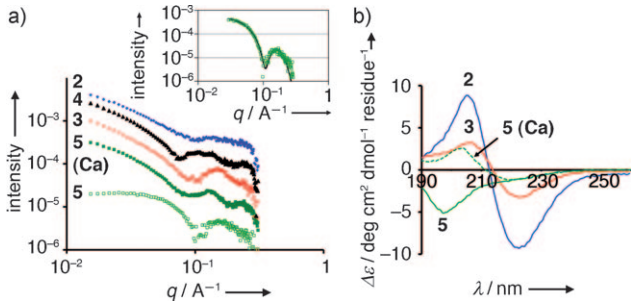

Figure 2. a) SAXS spectra of synthesized PA molecules (1 wt%) dissolved in salt solutions containing 150 mM NaCl, 3 mM KCl, and when noted, 5 mM $CaCl_2$. Curves were shifted vertically for visual convenience. Inset: Fit of **5** to a spherical-micelle model. b) CD curves of PAs (1 wt%) dissolved in the same salt solutions.

simulations is 9.7 nm. The reduction in fiber diameter from **1** to **2** suggests that the hydrophobic IKVAV epitopes are interdigitated and form antiparallel β sheets with the VVAA core of neighboring fibers.

When three glutamic acid residues were incorporated into the charged region, a mixture of interdigitated assemblies was observed. CryoTEM and conventional TEM (Figure 1b,f) showed that **3** assembled into a mixture of trimeric ribbons with fiber diameters of (7.1 ± 1) nm and cylindrical assemblies with a diameter of (12.8 ± 1.3) nm. For the trimer-ribbon motif, this increase in radius of approximately 0.5 nm from **2** to **3** corresponds closely to the simulated increase in molecular length upon the addition of an amino acid (ca. 0.4 nm). The structure that appears as a cylindrical assembly does not correspond to a conventional cylindrical aggregate; the diameter is larger than that expected from molecular simulations (10.4 nm), and there is a helical twist of 8–12° along the vertical axis of the fiber (Figure 1f, inset). These features support the notion that this supramolecular assembly is larger than two molecules. The difficulty in preparing solutions containing only cylindrical assemblies prevents elucidation of the structure from NMR spectroscopy. PA **4**, which contains an additional glycine residue between the charged EEE and the IKVAV segments, also forms a mixture of aggregated fibers, including bundled dimers (see Figure S2c) consisting of fibers of (8.1 ± 1.0) nm in diameter, triple helices (see Figure S2d) comprised of fibers of (7.7 ± 0.9) nm in diameter, and larger aggregates (see Figure 1c,g).

To disrupt interdigitation, a fourth glutamic acid residue was added to the negatively charged domain to give **5**. Surprisingly, this additional charged amino acid disrupted β-sheet formation and prevented self-assembly into nanofibers under conditions without appropriate screening. Only spherical micelles (see Figure S2e) with a diameter of (5.3 ± 1.1) nm were observed in CryoTEM micrographs of **5** (Figure 1d, inset). Furthermore, the SAXS curve can be fit to a core–shell spherical-micelle model with a diameter of (5.7 ± 1.2) nm (Figure 2a inset; see also Figure S5). Dynamic light scattering (DLS) confirmed further that solutions contained spherical micelles with a hydrodynamic radius of 8.6 nm. The lack of positive ellipticity in the CD spectrum indicates that **5** has a random-coil peptide structure in the supramolecular aggregates it forms (Figure 2b). There is also no β-sheet peak at 4.7 Å in the wide-angle X-ray scattering (WAXS) curve (see Figure S6). However, when a 1 wt% solution was drop-cast and dried on a TEM grid, cylindrical nanofibers with an average diameter of (10.8 ± 1.5) nm were the only structures observed (Figure 1h). This diameter corresponds to 88% of twice the simulated extended length of the molecule. The change in supramolecular structure is probably the result of an increase in concentration of the PA and salt impurities during the drying process involved in the preparation of the TEM grid. This observation suggests that assembly of **5** into cylindrical nanostructures can occur when the charges on the glutamic acid residues are properly screened. Indeed, when divalent $CaCl_2$ (5 mM) was added to the isotonic salt solution, cryoTEM revealed the existence of cylindrical structures with a diameter of (9.9 ± 1.1) nm (Figure 1d). Furthermore, the CD spectrum became positive at 210 nm, which indicated the presence of β-sheet structure (Figure 2b). A weak β-sheet peak at 4.7 Å was also observed in the WAXS spectrum (see Figure S6). The addition of calcium is physiologically relevant, as the cerebrospinal fluid of the nervous system contains Ca^{2+} at a concentration of 1.05–1.35 mM.[11] No significant change in morphology was observed by SAXS or cryoTEM for **1**–**4** when $CaCl_2$ (5 mM) was added to the isotonic salt solution.

To assess the ability of the molecules to promote neurite outgrowth, we quantified the average neurite length from neurons cultured in gels composed of networks of the filamentous structures formed by PAs **1**–**5**. Pluripotent murine P19 embryonal carcinoma cells were differentiated into neurons. These neurons were then homogeneously distributed into isotonic salt solutions composed of **1** (0.8 wt%) mixed with **2**–**5** (0.2 wt%) and gelled with $CaCl_2$ (25 mM). After culture for two days, the cells were fixed, and the neurites and nuclei were fluorescently labeled green and blue by β-III-tubulin immunostaining and Hoechst staining, respectively, then imaged by confocal microscopy (Figure 3a,b). Neurites were traced and measured, and average neurite lengths were calculated (Figure 3c). Surprisingly, we did not observe enhancement of neurite outgrowth when neurons were cultured in networks formed by **2**. However, in networks formed by PAs with additional glutamic acid residues in the charged domain of the peptide, neurite outgrowth was significantly increased. Cells cultured in gels containing **3** and **5** (0.2 wt%) revealed a (42 ± 13)% and (88 ± 13)% increase in neurite outgrowth, respectively.

The results of this study demonstrate that the surface display of the IKVAV sequence in supramolecular filaments is critical for strong bioactivity. IKVAV-bearing nanostructures that were less likely to form interdigitated bundles of cylindrical fibers (**3**, **5**) promoted neurite outgrowth, whereas those that bundled (**2**, **4**) did not. Less bundling of fibers and thus less masking of the IKVAV epitopes from receptors leads to a higher effective concentration of IKVAV epitopes available for binding. To test whether the concentration of the epitope affected neurite outgrowth, we also assayed gels containing half the concentration (0.1 wt%) of **5**. An increase in neurite length of (57 ± 14)% was observed: slightly more than half the effect observed in gels with 0.2 wt% of **5**

 © 2011 Wiley-VCH Verlag GmbH & Co. KGaA, Weinheim

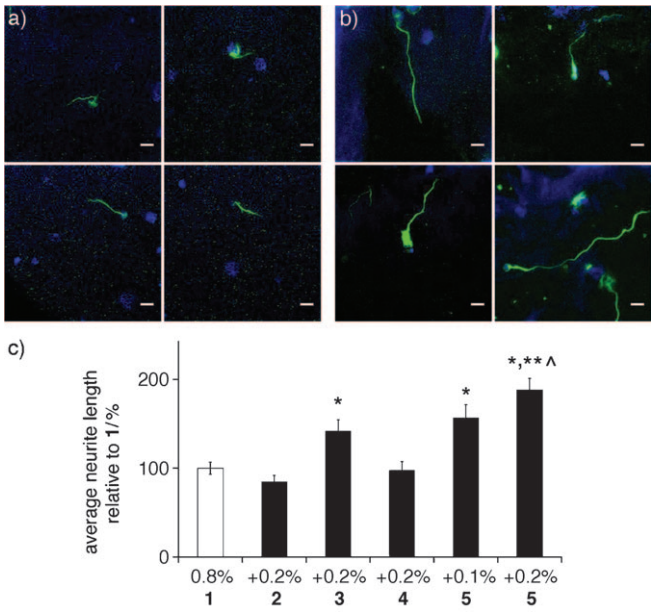

Figure 3. Representative flattened-stack confocal fluorescence images of neurons cultured in peptide-amphiphile gels containing **1** (0.8 wt%) with a) **2** (0.2 wt%) and b) **5** (0.2 wt%), as revealed by β-III-tubulin immunostaining (green) and Hoechst staining (blue). Scale bars: 20 μm. c) Average neurite lengths of neurons cultured in peptide-amphiphile gels. The amounts of the PAs added are given in wt%. $n > 59$; $*p < 0.01$ to **1**, $**p < 0.05$ to **3**.

(Figure 3c). This result further supports the notion that **5**, and to a lesser degree **3**, by forming less aggregated, cylindrical nanostructures, present higher effective concentrations of IKVAV epitopes capable of interacting with target receptors. We considered whether surface area determines the concentration of IKVAV available for binding and estimated the dimer and trimer bundles to have 63 and 52% of the surface area per unit length relative to isolated nanofibers (see the Supporting Information). That 0.1 wt% of **5** still produced a significant enhancement in neurite outgrowth, whereas 0.2 wt% of **2** and **4** did not, suggests that the IKVAV segment in **5** is also more effective at binding to receptors. Since **4**, which has the same molecular length as **5**, did not show any bioactivity, we can conclude that the enhanced coulombic repulsion in **5** is essential to prevent inter- and intrafiber β-sheet formation between neighboring IKVAV epitopes and thus foster a better interaction with the target receptor.

In summary, we have demonstrated that PA nanofibers that display a hydrophobic epitope, such as IKVAV, on their surface have a high propensity to interdigitate into bundles. This bundling naturally decreases the bioactivity of these self-assembling materials. We have also shown that nanofiber bundling can be suppressed by electrostatic forces. Our results demonstrate that the design of bioactive materials requires not only the incorporation of molecular signals, but also strategies to control the effective display of these signals on the nanoscale.

Received: January 10, 2011
Published online: May 30, 2011

Keywords: aggregation · biological activity · nanostructures · peptides · self-assembly

[1] a) M. P. Lutolf, J. A. Hubbell, *Nat. Biotechnol.* **2005**, *23*, 47; b) A. E. Nel, L. Madler, D. Velegol, T. Xia, E. M. V. Hoek, P. Somasundaran, F. Klaessig, V. Castranova, M. Thompson, *Nat. Mater.* **2009**, *8*, 543; c) M. J. Webber, J. A. Kessler, S. I. Stupp, *J. Intern. Med.* **2009**, *267*, 71.
[2] L. C. Palmer, S. I. Stupp, *Acc. Chem. Res.* **2008**, *41*, 1674.
[3] a) L. L. Kiessling, J. E. Gestwicki, L. E. Strong, *Angew. Chem.* **2006**, *118*, 2408; *Angew. Chem. Int. Ed.* **2006**, *45*, 2348; b) T. Muraoka, C.-Y. Koh, H. Cui, S. I. Stupp, *Angew. Chem.* **2009**, *121*, 6060; *Angew. Chem. Int. Ed.* **2009**, *48*, 5946.
[4] a) H. Cui, M. J. Webber, S. I. Stupp, *Biopolymers* **2010**, *94*, 1; b) J. D. Hartgerink, E. Beniash, S. I. Stupp, *Science* **2001**, *294*, 1684; c) Y.-C. Yu, P. Berndt, M. Tirrell, G. B. Fields, *J. Am. Chem. Soc.* **1996**, *118*, 12515.
[5] G. A. Silva, C. Czeisler, K. L. Niece, E. Beniash, D. A. Harrington, J. A. Kessler, S. I. Stupp, *Science* **2004**, *303*, 1352.
[6] V. M. Tysseling-Mattiace, V. Sahni, K. L. Niece, D. Birch, C. Czeisler, M. G. Fehlings, S. I. Stupp, J. A. Kessler, *J. Neurosci.* **2008**, *28*, 3814.
[7] a) M. C. Kibbey, M. Jucker, B. S. Weeks, R. L. Neve, W. E. Van Nostrand, H. K. Kleinman, *Proc. Natl. Acad. Sci. USA* **1993**, *90*, 10150; b) M. C. Kibbey, B. Johnson, R. Petryshyn, M. Jucker, H. K. Kleinman, *J. Neurosci. Res.* **1995**, *42*, 314.
[8] a) C. A. Kim, J. M. Berg, *Nature* **1993**, *362*, 267; b) M. Levitt, *Biochemistry* **1978**, *17*, 4277.
[9] M. Yamada, Y. Kadoya, S. Kasai, K. Kato, M. Mochizuki, N. Nishi, N. Watanabe, H. K. Kleinman, Y. Yamada, M. Nomizu, *FEBS Lett.* **2002**, *530*, 48.
[10] a) K. Saha, E. F. Irwin, J. Kozhukh, D. V. Schaffer, K. E. Healy, *J. Biomed. Mater. Res. Part A* **2007**, *81 A*, 240; b) Y. W. Tong, M. S. Shoichet, *Biomaterials* **2001**, *22*, 1029.
[11] S. V. Smith, D. T. Forman, *Clin. Lab. Sci.* **1994**, *7*, 32.

 © 2011 Wiley-VCH Verlag GmbH & Co. KGaA, Weinheim